Supporting Information

Investigating the Transformations of Polyoxoanions Using Mass Spectrometry and Molecular Dynamics

Jamie M. Cameron,[a,c] Laia Vilà-Nadal,[a] Ross S. Winter,[a] Fumichika Iijima,[c] Juan Carlos Murillo,[b] Antonio Rodríguez-Fortea[b], Hiroki Oshio,[c] Josep M. Poblet*[b] and Leroy Cronin*[a]

[a] *WestCHEM, School of Chemistry, The University of Glasgow, Glasgow, UK, G12 8QQ.*

[b] *Departament de Química Física i Inorgànica, Universitat Rovira i Virgili, C/ Marcel·lí Domingo 1, 43007 Tarragona, Spain*

[c] *Department of Chemistry, Graduate School of Pure and Applied Sciences,*

University of Tsukuba, Tennodai 1-1-1, Tsukuba 305-8571, Japan

E-mail: josepmaria.poblet@urv.cat; Lee.Cronin@glasgow.ac.uk

Materials, Physical Measurements and Computational Details

All reagents were purchased commercially from *Sigma Aldrich* or *Alfa Aesar* and used without further purification. HPLC grade solvents were purchased from *Fisher Scientific* and used as received.

$K_8[\beta_2\text{-}SiW_{11}O_{39}]^{\cdot}14H_2O$ was synthesized according to the previously reported procedure.[1]

Synthesis of $K_8[\gamma\text{-}SiW_{10}O_{36}]^{\cdot}12H_2O$: The synthesis of $K_8[\gamma\text{-}SiW_{10}O_{36}]^{\cdot}12H_2O$ was performed following the previously reported method by Canny *et al.*, at one quarter scale.[2] $K_8[\beta_2\text{-}SiW_{11}O_{39}]^{\cdot}14H_2O$ (7.5 g) was dissolved with stirring in 75 mL of H_2O and the pH was then adjusted to 9.1 by addition of 2 M K_2CO_3 solution. During the reaction time (20 minutes), the pH was carefully maintained at this value by further addition of 0.1 M K_2CO_3 solution before the addition of 10 g solid KCl was used to precipitate the final product as a fine white powder.

The identity of product could be confirmed by subsequent IR analysis of the dried powder.

Preparation of Samples for Time Resolved Mass Spectrometry Solutions for ESI-MS analysis were prepared by removing 20 µL aliquots of the reaction mixture prior to, following and at timed intervals during the reaction before immediately diluting in a clean glass vial with an additional 1 mL of H_2O. Each solution was then well-mixed prior to their subsequent introduction to the spectrometer.

Electrospray Ionization Mass Spectrometry (ESI-MS) was performed on a Waters Synapt-G2 HDMS spectrometer operating in sensitivity mode, equipped with a quadrupole and time of flight (Q/ToF) module for MS analysis. All samples were prepared as described above and injected directly at a flow rate of 5 µL min^{-1} using a *Harvard* syringe pump. All spectra were collected in negative ion mode and subsequently analysed using the *Waters* MassLynx v4.1 software.

For all measurements the following parameters were employed: capillary voltage: 1.65 kV; sample cone voltage: 30 V; extraction cone voltage: 4.5 V; source temperature: 80 ˚C; desolvation temperature: 120 ˚C; cone gas flow: 20 L h^{-1} (N_2); desolvation gas flow: 500 L h^{-1} (N_2).

Computational details and relevant references are provided in the main manuscript text. Static Density Functional Theory (DFT) calculations and Classical Molecular Dynamics (CMD) simulations were performed in *in-house computational facilities* in the Quantum Chemistry Group in Tarragona (Spain). Carr Parrinello Molecular Dynamics (CPMD) simulations were performed in the Barcelona Supercomputing Center (BSC).

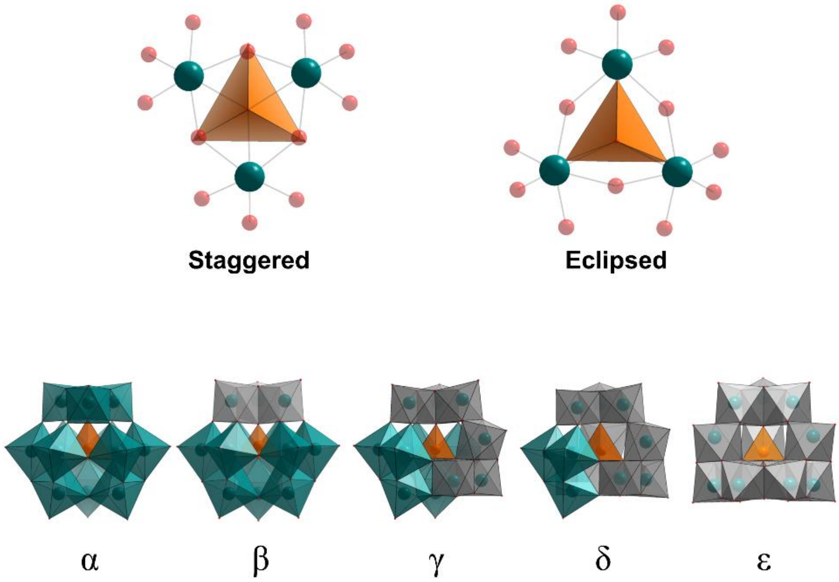

Figure S1. Depiction of the geometrical isomerism possible within the Keggin cluster archetype which occurs *via* subsequent 60° rotations of each of the four individual {M_3} triads present in the structure along their three-fold axis. This results in the theoretical existence of five possible isomers which can be distinguished structurally, most easily by considering the conformation of the individual {M_3} triads whereby a rotated group adopts an eclipsed configuration relative to the central heteroatom rather than the native staggered conformation (top). This gives rise to the five, theoretically possible geometric isomers of the Keggin cluster (shown bottom, rotated triads highlighted in grey). Note that the isomerism event which is the focus of our attention in this work occurs between the β- and γ-isomers.

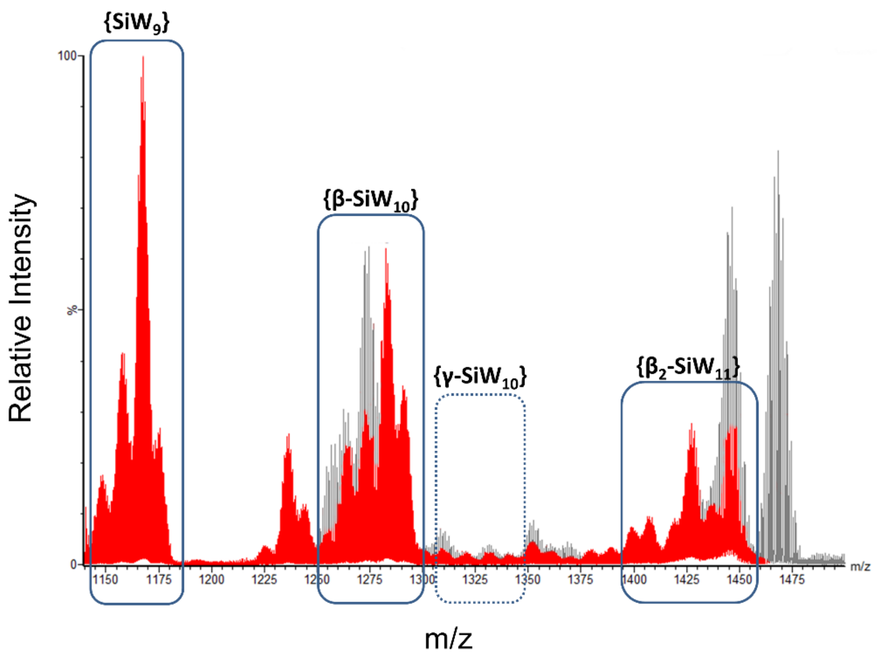

Figure S2: ESI-MS spectrum of the β-SiW_{11} starting material dissolved in water prior to addition of base and the notional start-point of the reaction. Red envelopes highlight the peaks corresponding to the highlighted anions and grey envelopes represent smaller, singly charged cluster fragments caused by in-source fragmentation and decomposition.

Table S1: Comparison of peak assignments obtained during standard measuring conditions (optimized for both peak intensity and analyte stability) and those obtained under a higher cone voltage setting (in which greater in-source fragmentation may occur). In all cases, the intensity of the signals decreases upon increased source settings to the point where several can no longer be detected in the spectrum, indicating their fragmentation to smaller species. This suggests that these species are originating predominantly from solution rather than in-source effects and may therefore be taken as representative of the solution composition. In both series of measurements, spectrometer settings are as described in the methods section above, where only the sample cone voltage has been increased to 55 V in the higher mode settings.

				Standard Settings	**High Settings**
Anion	*z*	Assignment	*m/z* (calc)	*m/z* (obs)	*m/z* (obs)
{SiW$_9$}	2-	{$NaH_7[SiW_9O_{34}]$}	1128.7	1128.6	1128.6
	2-	{$Na_2H_6[SiW_9O_{34}]\cdot H_2O$}	1148.7	1148.7	1148.7*
	2-	{$KNaH_6[SiW_9O_{34}]\cdot H_2O$}	1156.7	1156.6	1156.6*
	2-	{$KNa_2H_5[SiW_9O_{34}]$}	1158.7	1158.6	-
	2-	{$KNa_2H_5[SiW_9O_{34}]\cdot H_2O$}	1167.7	1167.6	-
	2-	{$K_2NaH_5[SiW_9O_{34}]\cdot H_2O$}	1175.7	1175.6	-
{β-SiW$_{10}$}	2-	{$NaH_7[SiW_{10}O_{37}]$}	1244.7	1244.6	1245.0
	2-	{$NaH_7[SiW_{10}O_{37}]\cdot H_2O$}	1253.7	1254.1	1253.2*
	2-	{$Na_2H_6[SiW_{10}O_{37}]\cdot H_2O$}	1264.7	1264.6	-
	2-	{$KNaH_6[SiW_{10}O_{37}]\cdot H_2O$}	1272.7	1273.1	1273.1*
	2-	{$KNa_2H_5[SiW_{10}O_{37}]\cdot H_2O$}	1283.6	1283.5	-
	2-	{$K_2NaH_5[SiW_{10}O_{37}]\cdot H_2O$}	1291.6	1291.5	1291.1*
{γ-SiW$_{10}$}**	2-	{$K_3Na_2H[SiW_{10}O_{36}]\cdot H_2O$}	1312.6	-	1313.1
	2-	{$K_5H[SiW_{10}O_{36}]$}	1319.6	1319.5	-
	2-	{$K_5Na[SiW_{10}O_{36}]$}	1330.6	1330.5	-
	2-	{$K_3Na_3[SiW_{10}O_{36}]\cdot 2H_2O$}	1332.6	-	1332.6
	2-	{$K_6[SiW_{10}O_{36}]$}	1338.5	1338.5	-
	2-	{$K_3Na_3[SiW_{10}O_{36}]\cdot 3H_2O$}	1341.6	-	1341.6
{β-SiW$_{11}$}	2-	{$KNa_2H_3[SiW_{11}O_{39}]\cdot 2H_2O$}	1399.6	1399.5	1399.5
	2-	{$K_3NaH_2[SiW_{11}O_{39}]$}	1408.6	1408.5	1408.1
	2-	{$K_3Na_2H[SiW_{11}O_{39}]$}	1419.6	1419.5	1419.1*
	2-	{$K_4NaH[SiW_{11}O_{39}]$}	1427.5	1427.5	1428.1

* Note that these peaks are low intensity, poorly resolved and often obscured by overlapping singly charged fragments. Their assignment is therefore tentative and only for comparison to those made under optimized source settings (i.e. standard settings).

** It is interesting to note that, whilst none of the signals observed under ideal conditions are readily identifiable under the higher source settings for {γ-SiW$_{10}$}, relatively well resolved envelopes corresponding to different mixed cation salts can be assigned in the same region of the spectrum (as shown above). This phenomena is not unexpected and arises as a result of the different ionization characteristics of each cluster under these conditions. Similar signals can be observed for {β-SiW$_{11}$} in particular, but will not be described here.

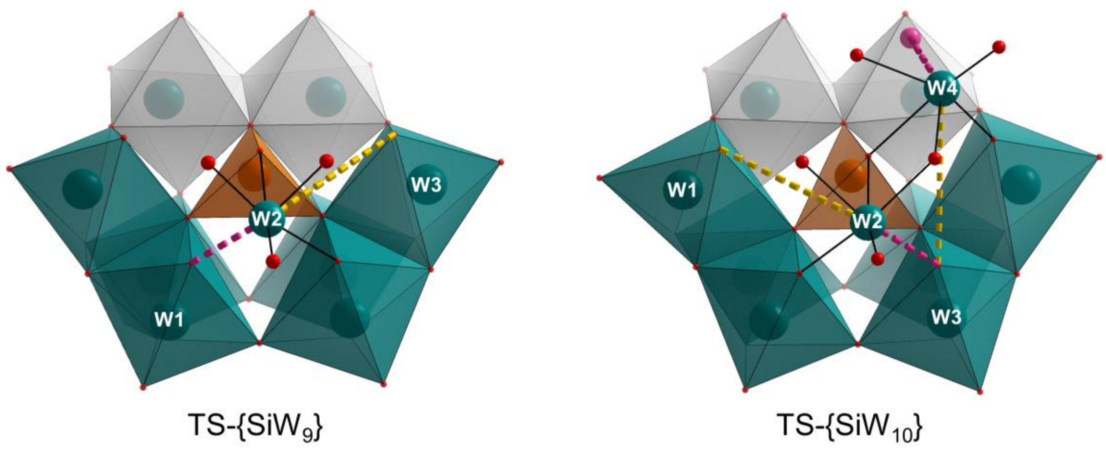

Figure S3. Hypothesized transition states for the β- to γ- isomerization of the {SiW_9} (left) and {SiW_{10}} (right) intermediates. Dashed lines indicate bond formation (shown in yellow) and bond breaking (pink) respectively, whilst bonds which retain their original connectivity are shown as solid lines. Note that the oxygen atom highlighted in pink present in the {SiW_{10}} transition state is lost upon completion of the β- to γ- transformation. Colour code: W = teal, Si = orange, O = red.

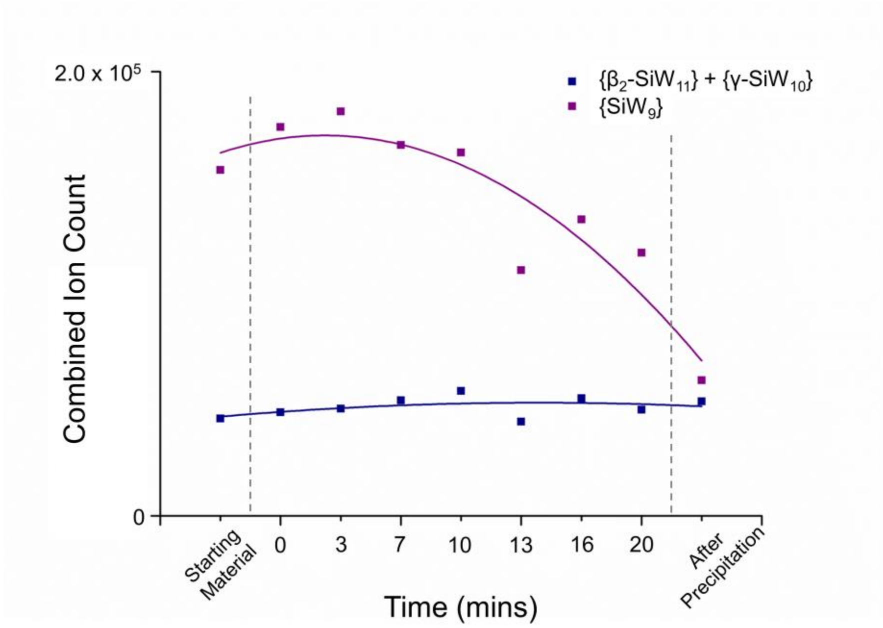

Figure S4: Plot of combined ion count (CIC) values for the sum of both β_2-SiW_{11} starting material and γ-SiW_{10} product *vs.* the proposed SiW_9 intermediate. The respective profiles of both plots suggests that the observed abundance of SiW_9 species is genuinely time-dependent and thus has a mechanistic origin rather than arising as a product of the measurement technique (*i.e.* the observed abundance is not governed by the relative amounts of either starting material or product present at any given point in the reaction coordinate). The dashed vertical lines on the plot indicate the point in the reaction coordinate at which either base (left) or KCl (right) is added. The lines of best fit are provided primarily as a guide for the eye.

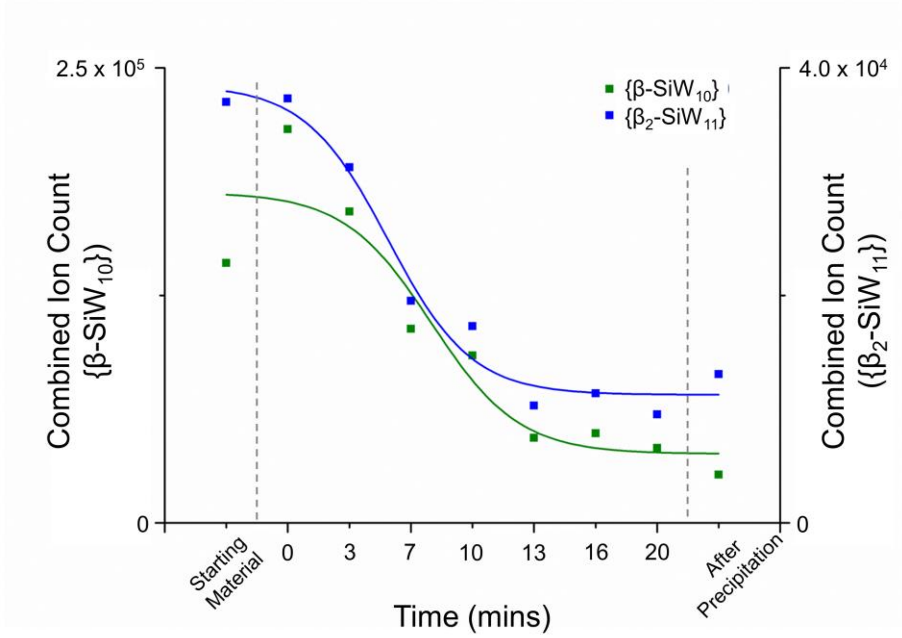

Figure S5: Plot of combined ion count (CIC) values for the β-SiW_{11} starting material *vs*. the β-SiW_{10} fragment. The close match between the profiles of both traces help to indicate that the β-SiW_{10} fragment is likely to be a direct product of the fragmentation of the starting material. The dashed vertical lines on the plot indicate the point in the reaction coordinate at which either base (left) or KCl (right) is added. The lines of best fit are provided primarily as a guide for the eye.

Table S2. Frontier Orbital Energies for Several Polyoxotungstates. Energies given in eV.

Anion	E(HOMO)	E(LUMO)	H-L gap
α-SiW_{12}	-6.89	-4.19	2.70
β-SiW_{12}	-6.86	-4.34	2.52
β-SiW_{11}	-5.68	-2.96	2.72
β-SiW_9	-4.85	-2.04	2.81
γ-SiW_9	-4.84	-2.04	2.80
γ-SiW_{10}	-5.60	-2.74	2.86
β-SiW_{11}-K	-5.77	-3.03	2.74
β-SiW_9-K	-4.88	-2.10	2.78
γ-SiW_9-K	-4.96	-2.12	2.84
γ-SiW_{10}-K	-5.67	-2.82	2.84

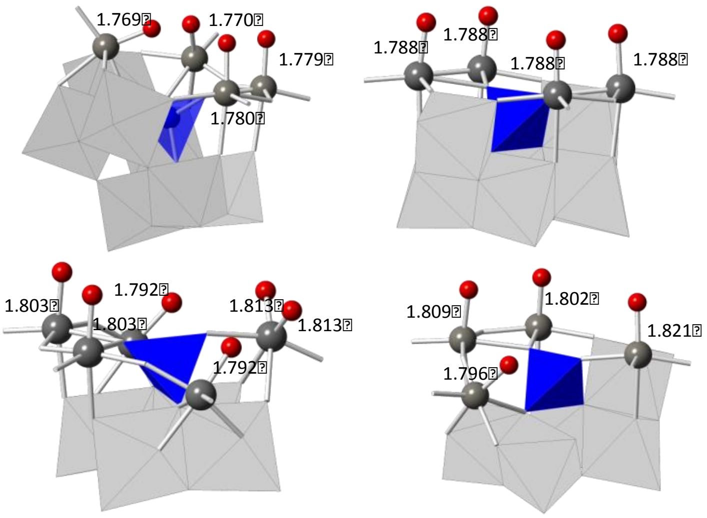

Figure S6. Structures computed for anions [β-$SiW_{11}O_{39}$]$^{8-}$, [β-SiW_9O_{34}]$^{10-}$, [γ-SiW_9O_{34}]$^{10-}$ and [γ-$SiW_{10}O_{36}$]$^{8-}$.

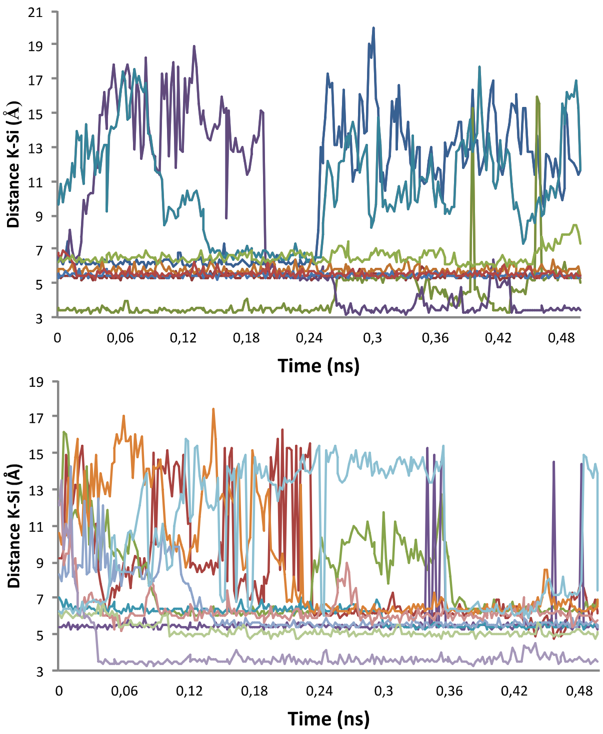

Figure S7. K-Si distances for the 10 K^+ ions for the trivacant K_{10}[β-SiW_9O_{34}] (top) and K_{10}[γ-SiW_9O_{34}] (bottom) systems along 0.5 ns of classical MD trajectories.

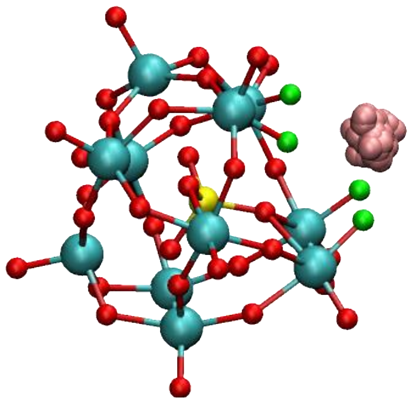

Figure S8. Representation of the motion of the K^+ near the vacancy for a 20 ps Car-Parrinello MD trajectory of $[\beta\text{-}SiW_{11}O_{39}]^{8-}$. No protonation of the polyanion is observed during the trajectory.

(a)

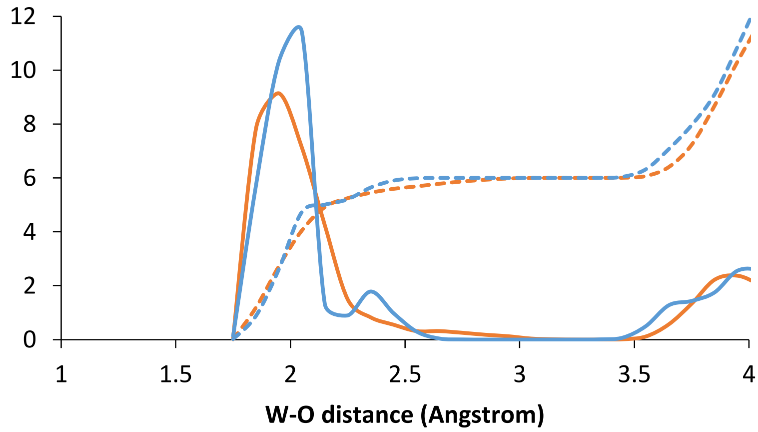

(b)

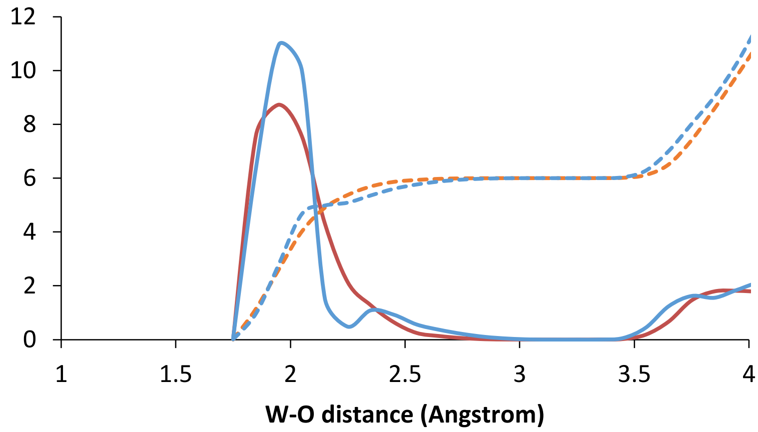

Figure S9. W-O radial distribution functions (solid lines) and their integrations, the coordination number (broken line), for (a) the five W atoms near the lacuna (red) and for the remaining four W atoms (blue) of the tri-lacunary $[\beta\text{-}SiW_9O_{34}]^{10-}$, obtained from Car-Parrinello MD trajectory (5 ps); (b) the four W atoms near the lacuna (red) and for the remaining five W atoms (blue) of the tri-lacunary $[\gamma\text{-}SiW_9O_{34}]^{10-}$, obtained from Car-Parrinello MD trajectory (5 ps).

(a)

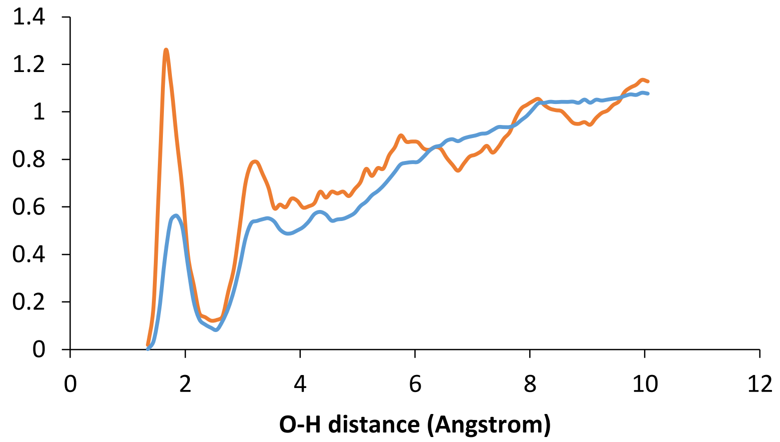

(b)

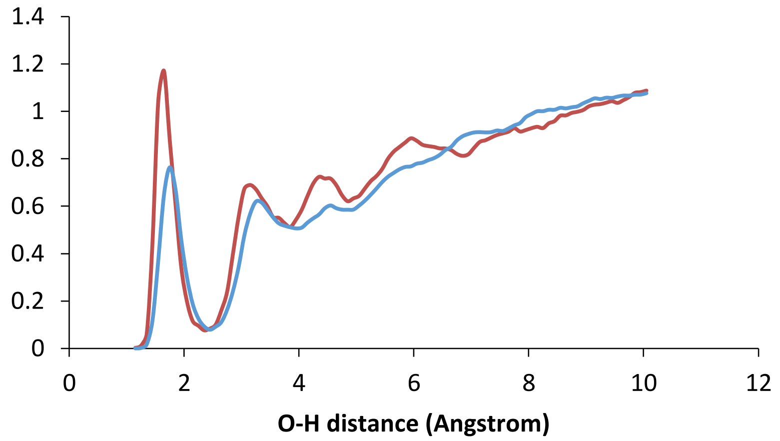

Figure S10. O-H radial distribution functions for (a) the five terminal O atoms in the lacuna (red) and for the remaining O atoms (blue) of the tri-lacunary $[\beta\text{-}SiW_9O_{34}]^{10-}$, obtained from Car-Parrinello MD trajectory (5 ps); (b) the four terminal O atoms in the lacuna (red) and for the remaining O atoms of the tri-lacunary $[\gamma\text{-}SiW_9O_{34}]^{10-}$, obtained from Car-Parrinello MD trajectory (5 ps).

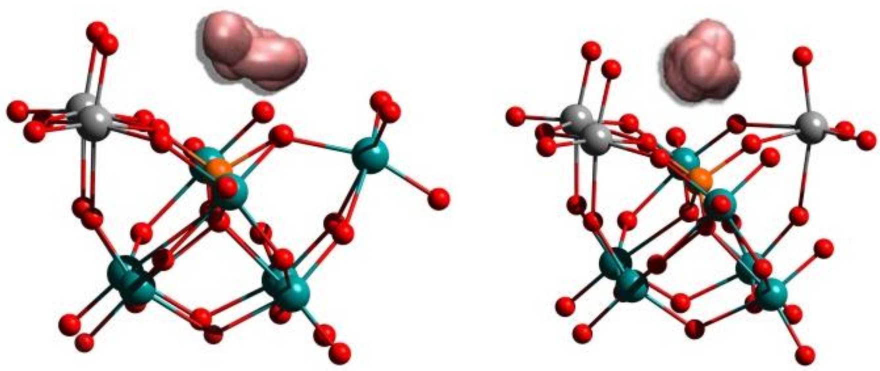

Figure S11. The motion of the K^+ ion closer to the lacuna $K_{10}[\beta\text{-}SiW_9O_{34}]$ and $K_{10}[\gamma\text{-}SiW_9O_{34}]$ systems during the Car-Parrinello trajectories. Colour code: W = teal, Si = orange, O = red. Grey is used to differentiate W-centres belonging to rotated $\{W_3\}$ triads.

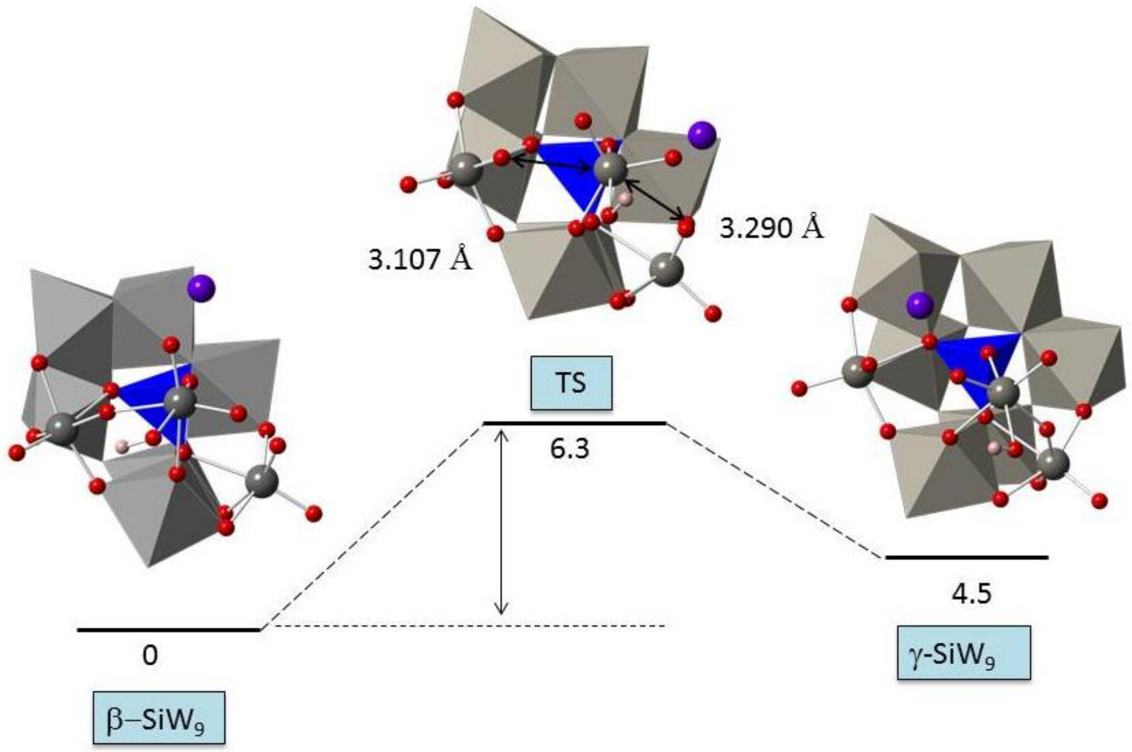

Figure S12. Energy profile (in kcal·mol^{-1}) for the monoprotonated {β-SiW$_9$} to {γ-SiW$_9$} transformation, the transition state (TS) structure.

Table S3. xyz coordinates for the optimized structure of γ-SiW9

γ-SiW9			
1.K	-0.720655	0.940855	-3.736331
2.Si	0.057021	-0.150724	-0.690767
3.W	-1.619979	-2.452025	-2.645525
4.W	-3.495379	0.324659	-0.418010
5.W	2.214068	2.742726	-1.079434
6.W	3.622526	-0.774572	-0.802086
7.W	2.293342	0.591487	2.086974
8.W	-1.993814	-2.150602	1.297711
9.W	-1.507094	1.174008	2.292669
10.W	1.671622	-2.774843	1.186182
11.W	-1.142563	3.238419	-0.927750
12.O	-0.234941	-1.115794	-1.977428
13.O	-1.264929	-0.212104	0.323687
14.O	0.216918	1.410574	-1.209661
15.O	1.421572	-0.655891	0.131005
16.O	-0.146176	-2.490600	1.836495
17.O	0.332361	0.733989	2.613745
18.O	-2.609016	1.967895	-1.059475
19.O	2.964704	-1.535874	-2.283674
20.O	-1.016316	2.557760	1.123188
21.O	1.139015	-3.639709	-0.281703
22.O	1.987221	2.065399	0.918606
23.O	-1.713838	-2.851204	-0.383335
24.O	3.195943	1.058565	-1.322489
25.O	-2.991522	-0.580168	-1.928021
26.O	-2.012296	-0.723091	2.732550
27.O	-1.129248	3.516045	-2.716638
28.O	2.170346	-1.263752	2.601759
29.O	-0.544760	-3.863031	-2.946088
30.O	0.694394	3.914840	-0.613351
31.O	3.452999	-2.335026	0.374121
32.O	-3.275022	1.205763	1.403080
33.O	-3.697356	-1.303402	0.639075
34.O	3.870859	0.192389	1.120103
35.O	-1.669723	-1.663705	-4.289065
36.O	2.048274	2.956838	-2.866108
37.O	-3.260459	-3.256777	-2.586614
38.O	-5.211869	0.740921	-0.717366
39.O	3.548660	3.869220	-0.667444
40.O	5.395689	-0.804892	-1.086226
41.O	2.979166	1.359981	3.555206
42.O	-2.792472	-3.477075	2.206026
43.O	-1.936452	2.009124	3.819406
44.O	2.206251	-4.100787	2.275621
45.O	-2.010842	4.702780	-0.350984

Table S4. xyz coordinates for the optimized structure of β-SiW9

β-SiW9			
1.K	-1.496965	0.776263	-3.480122
2.Si	-0.014971	-0.035168	-0.720186
3.W	-0.727699	-2.979259	-2.397785
4.W	-3.685282	0.643599	-0.330910
5.W	2.181049	2.737876	-1.103710
6.W	3.499089	-0.821747	-0.944861
7.W	2.256253	0.493083	2.021307
8.W	-2.176880	-2.008386	1.206270
9.W	-1.490714	1.221230	2.326779
10.W	1.455963	-2.799499	0.989426
11.W	-1.101021	3.398493	-0.797669
12.O	-0.276208	-0.999106	-2.005373
13.O	-1.359525	-0.071996	0.273577
14.O	0.206969	1.535765	-1.208996
15.O	1.351242	-0.565151	0.063311
16.O	-0.349864	-2.508830	1.689063
17.O	0.346664	0.607207	2.578752
18.O	-2.652167	2.214697	-0.898543
19.O	2.833655	-1.417639	-2.489764
20.O	-0.911682	2.613434	1.207520
21.O	0.722511	-3.283274	-0.629447
22.O	2.041445	2.036990	0.995023
23.O	-1.954298	-2.671918	-0.492350
24.O	3.128565	1.062524	-1.366568
25.O	-3.548101	-0.097230	-1.971061
26.O	-2.062511	-0.665769	2.704492
27.O	-1.140749	3.691919	-2.581091
28.O	2.062391	-1.504517	2.389047
29.O	0.630536	-3.249548	-3.557995
30.O	0.759133	3.977805	-0.515101
31.O	3.226189	-2.465279	0.086770
32.O	-3.260620	1.410731	1.576134
33.O	-3.853696	-1.032836	0.635238
34.O	3.805382	0.007383	1.034734
35.O	-2.071829	-2.498666	-3.511745
36.O	2.045981	3.097864	-2.858281
37.O	-1.182400	-4.725009	-2.043249
38.O	-5.369843	1.251997	-0.322156
39.O	3.553383	3.790903	-0.614426
40.O	5.272254	-0.898635	-1.221374
41.O	3.001287	1.061758	3.552264
42.O	-3.055607	-3.310643	2.075508
43.O	-1.753703	2.007332	3.917450
44.O	1.873244	-4.352568	1.774998
45.O	-1.876353	4.886216	-0.156581

Table S5. xyz coordinates for the optimized structure of TS-SiW9

TS-SiW9			
1.K	-1.388494	0.850451	-3.525904
2.Si	0.023444	-0.083687	-0.694519
3.W	-1.124021	-2.772761	-2.585612
4.W	-3.637783	0.523776	-0.364417
5.W	2.189818	2.713728	-1.097546
6.W	3.553750	-0.819638	-0.863031
7.W	2.270538	0.530935	2.053668
8.W	-2.047940	-2.036741	1.223562
9.W	-1.500966	1.220108	2.316806
10.W	1.587032	-2.807876	1.119917
11.W	-1.122726	3.343789	-0.845468
12.O	-0.259425	-1.030733	-1.995206
13.O	-1.319386	-0.105782	0.294493
14.O	0.208661	1.478151	-1.203458
15.O	1.370775	-0.644286	0.110736
16.O	-0.227829	-2.475812	1.763122
17.O	0.334103	0.679287	2.592579
18.O	-2.655615	2.130751	-0.931511
19.O	2.875188	-1.552387	-2.347367
20.O	-0.968616	2.621699	1.190761
21.O	0.973477	-3.605812	-0.366894
22.O	1.993941	2.029175	0.926481
23.O	-1.732047	-2.686563	-0.494735
24.O	3.133128	1.022072	-1.377571
25.O	-3.418845	-0.245069	-1.983654
26.O	-2.031055	-0.704455	2.703352
27.O	-1.155369	3.599782	-2.634798
28.O	2.130185	-1.351669	2.535868
29.O	0.344017	-3.529837	-3.282307
30.O	0.728418	3.950290	-0.569060
31.O	3.355374	-2.404845	0.281153
32.O	-3.272676	1.318193	1.535726
33.O	-3.759729	-1.157102	0.605168
34.O	3.835088	0.106734	1.061619
35.O	-1.899686	-1.964741	-4.003489
36.O	2.041193	3.025121	-2.866531
37.O	-2.214933	-4.245465	-2.444475
38.O	-5.344656	1.064214	-0.409871
39.O	3.556750	3.787279	-0.641207
40.O	5.323434	-0.871371	-1.160564
41.O	2.990994	1.245073	3.534818
42.O	-2.895304	-3.386026	2.052440
43.O	-1.829267	2.002233	3.895693
44.O	2.076329	-4.188293	2.156903
45.O	-1.929273	4.833046	-0.249972

References

1. Contant, R.; Tézé, A. *Inorganic Syntheses*; John Wiley & Sons,, Hoboken, NJ, USA 1990; Vol. 27.
2. Canny, J.; Tézé, A.; Thouvenot, R.; Hervé, G. *Inorg. Chem.* **1986**, *25*, 2114.